A&A, 687, A199 (2024)
https://doi.org/10.1051/0004-6361/202449536

Astronomy & Astrophysics

Thermonuclear ^{28}P(p, γ)^{29}S reaction rate and astrophysical implication in ONe nova explosion

J. B. Liu[1,2], J. José[3,4], S. Q. Hou[1,2,5], M. Pignatari[5,6,7,8,9], T. C. L. Trueman[5,6,7,8], R. Longland[10,11], J. G. Li[1,2], C. A. Bertulani[12], and X. X. Xu[1,2]

[1] Key Laboratory of High Precision Nuclear Spectroscopy, Institute of Modern Physics, Chinese Academy of Sciences, 509 Nanchang Rd, Lanzhou 730000, PR China
e-mail: sqhou@impcas.ac.cn
[2] School of Nuclear Science and Technology, University of Chinese Academy of Sciences, 19A Yuquan Rd, Shijingshan District, Beijing 100049, PR China
[3] Departament de Física, Universitat Politècnica de Catalunya, 08019 Barcelona, Spain
[4] Institut d'Estudis Espacials de Catalunya, Universitat Politècnica de Catalunya, 08034 Barcelona, Spain
[5] NuGrid Collaboration, http://www.nugridstars.org
[6] Konkoly Observatory, HUN-REN, H-1121 Budapest, Konkoly Thege M. út 15–17, Hungary
[7] CSFK, MTA Centre of Excellence, Budapest, Konkoly Thege Miklós út 15–17, 1121, Hungary
[8] E. A. Milne Centre for Astrophysics, University of Hull, Cottingham Rd, Kingston upon Hull HU6 7RX, UK
[9] Joint Institute for Nuclear Astrophysics – Center for the Evolution of the Elements, 640 S Shaw Lane, East Lansing, MI 48824, USA
[10] Department of Physics, North Carolina State University, Raleigh, NC 27695, USA
[11] Triangle Universities Nuclear Laboratory, Durham, NC 27708, USA
[12] Department of Physics and Astronomy, Texas A&M University-Commerce, Commerce, TX 75429, USA

Received 8 February 2024 / Accepted 11 April 2024

ABSTRACT

Context. An accurate ^{28}P(p, γ)^{29}S reaction rate is crucial to defining the nucleosynthesis products of explosive hydrogen burning in ONe novae. Using the recently released nuclear mass of ^{29}S, together with a shell model and a direct capture calculation, we reanalyzed the ^{28}P(p, γ)^{29}S thermonuclear reaction rate and its astrophysical implication.
Aims. We focus on improving the astrophysical rate for ^{28}P(p, γ)^{29}S based on the newest nuclear mass data. Our goal is to explore the impact of the new rate and associated uncertainties on the nova nucleosynthesis.
Methods. We evaluated this reaction rate via the sum of the isolated resonance contribution instead of the previously used Hauser-Feshbach statistical model. The corresponding rate uncertainty at different energies was derived using a Monte Carlo method. Nova nucleosynthesis is computed with the 1D hydrodynamic code SHIVA.
Results. The contribution from the capture on the first excited state at 105.64 keV in ^{28}P is taken into account for the first time. We find that the capture rate on the first excited state in ^{28}P is up to more than 12 times larger than the ground-state capture rate in the temperature region of 2.5×10^7 K to 4×10^8 K, resulting in the total ^{28}P(p, γ)^{29}S reaction rate being enhanced by a factor of up to 1.4 at $\sim 1 \times 10^9$ K. In addition, the rate uncertainty has been quantified for the first time. It is found that the new rate is smaller than the previous statistical model rates, but it still agrees with them within uncertainties for nova temperatures. The statistical model appears to be roughly valid for the rate estimation of this reaction in the nova nucleosynthesis scenario. Using the 1D hydrodynamic code SHIVA, we performed the nucleosynthesis calculations in a nova explosion to investigate the impact of the new rates of ^{28}P(p, γ)^{29}S. Our calculations show that the nova abundance pattern is only marginally affected if we use our new rates with respect to the same simulations but statistical model rates. Finally, the isotopes whose abundance is most influenced by the present ^{28}P(p, γ)^{29}S uncertainty are ^{28}Si, ^{33,34}S, ^{35,37}Cl, and ^{36}Ar, with relative abundance changes at the level of only 3% to 4%.

Key words. nuclear reactions, nucleosynthesis, abundances – stars: abundances – novae, cataclysmic variables

1. Introduction

Nova explosions stand out as relatively frequent cataclysmic events. They occur in interacting binary systems consisting of a white-dwarf and a main-sequence (or a red-giant) companion, with an estimated Galactic frequency of $\sim 50^{+31}_{-23}$ novae per year (Shafter 2017). It is worth noting that only a fraction of these events, around ten per year, are actually obscured by interstellar dust. In contrast to type Ia supernovae, neither the white dwarf nor the binary system is expected to be disrupted during a classical nova. In fact, novae constitute recurrent phenomena, exhibiting periodicities spanning between 10^4 and 10^5 yr. In the subclass of recurring novae (by definition, novae observed in outburst more than once), recurrence times vary from 1 to 100 yr. The question of whether these recurrence times constitute a nearly continuous sequence, encompassing the shorter values observed for recurrent novae and the longer periods predicted for classical novae, is still a matter of debate.

Classical novae are characterized by the ejection of approximately 10^{-7} to 10^{-4} $M_\odot$ of nuclear-processed material, at typical velocities exceeding 1000 km s^{-1} (Starrfield et al. 2008, 2016; José & Shore 2008; José et al. 2016). Spectral analysis has proven

instrumental in unraveling crucial details concerning the properties of expanding nova ejecta; it particularly sheds light on its chemical composition. Observationally, the nova ejecta exhibits significant amounts of carbon (C), nitrogen (N), and oxygen (O). In the case of ONe novae, which constitute approximately one-third of the total, there are discernible overabundances of additional elements, such as neon (Ne), as first reported by Gehrz et al. (1998). In fact, spectroscopic analyses have revealed that the inferred metallicity within the ejecta typically falls within the range of $Z \sim 0.2$–0.5. The origin of these metallicity enhancements in the ejecta remains unexplained, although prevailing hypotheses attribute them to mixing episodes occurring at the core-envelope boundary. Among the different mechanisms proposed to date, one of the most promising involves Kelvin-Helmholtz hydrodynamic instabilities within the context of 3D turbulent convection (Casanova et al. 2011; José et al. 2020). This dynamic framework offers a compelling explanation for the observed metallicity enhancements, providing a deeper understanding of the intricate processes underlying nova events. An alternative mechanism was recently proposed, which is based on deep, shear-driven mixing (Bellomo et al. 2024).

The main nuclear processes during nova outbursts involve proton captures, (p, γ) and (p, α), and β^+-decays, with the main nuclear path running close to the valley of stability. Current models for novae predict peak temperatures below 4×10^8 K, precluding the occurrence of α-capture reactions and the potential extension of the nuclear path through CNO breakout. Calcium (Ca) is thought to be the endpoint in nova nucleosynthesis (José et al. 2006, 2001). From a nuclear physics perspective, novae represent unique stellar explosions; the relatively confined nuclear activity, involving approximately one hundred species (below mass $A < 40$) linked through a few hundred nuclear processes, as well as the limited range of temperatures attained during the outburst, $T \sim 10^7$ to 4×10^8 K, allow us to rely primarily on experimental information (José et al. 2006).

Nova nucleosynthesis in the Si–Ca region is mainly governed by the ^{30}P(p, γ)^{31}S reaction (in competition with ^{30}P(β^+)^{30}Si), which determines the final ^{30}Si/^{28}Si ratio in the ejecta; this is a valuable tool for identifying presolar grains of a putative nova origin (Downen et al. 2012). Other reactions, such as ^{28}P$(p, \gamma)^{29}$S, also have an obvious influence on nova nucleosynthesis in this mass region. As pointed out by Iliadis et al. (2002) in a thorough sensitivity study, a ^{28}P$(p, \gamma)^{29}$S rate variation by a factor of 100 results in a noticeable change in the final abundances of ^{33,34}S, ^{35}Cl, and ^{36}Ar in some nova models, by factors between 0.92 and 1.4. Proton captures on ^{29}S cannot proceed in a nova explosion because of the –480 keV proton separation energy in ^{30}Cl. Thus, the reaction flow passing through ^{28}P is responsible for the synthesis of intermediate-mass elements in this region, either by ^{28}P$(p, \gamma)^{29}$S$(\beta^+)^{29}$P, or by ^{28}P$(\beta^+)^{28}$Si$(p, \gamma)^{29}$P. In light of this, accurate ^{28}P$(p, \gamma)^{29}$S rates are needed for a comprehensive understanding of the main nova nucleosynthesis path as well as for the abundance patterns of elements ranging from Si to Ca (José et al. 2001).

There currently exist four different rates for the ^{28}P$(p, \gamma)^{29}$S reaction in the literature. The earliest evaluation was presented by Wallace & Woosley (1981), but the method used to derive the rate was not clarified. Later, this rate was reevaluated by Rauscher & Thielemann (2000), Cyburt et al. (2010), and Sallaska et al. (2013) based on Hauser-Feshbach statistical estimates. It is well known that the statistical model is only applicable for the case of sufficient high-level density in the compound nucleus (Rauscher & Thielemann 2000; Cyburt et al. 2010). However, this condition is not met for ^{29}S, especially in the low-energy domain of nova interest. The reaction rate for nova nucleosynthesis is mainly determined by the near-threshold isolated resonances, and it is substantially influenced by the nuclear masses of the nuclei involved in the reaction. Therefore, for an arbitrary reaction, accurate nuclear masses are crucial for determining the reaction rates. For the ^{28}P$(p, \gamma)^{29}$S reaction, the Q values used in the previous four works are nearly identical: about 3290(50) keV (Rauscher & Thielemann 2000; Cyburt et al. 2010; Sallaska et al. 2013; Wallace & Woosley 1981). However, the recently released nuclear mass data of ^{28}P and ^{29}S in the evaluation of atomic mass (AME2020) (Wang et al. 2021) provides a highest precision reaction Q value of 3235(13) keV, which allows us to reduce the uncertainty of the reaction rates.

In order to verify whether the Hauser-Feshbach statistical model is suitable for the evaluation of this reaction rate, especially for the nova temperature domain, in this work we derive the ^{28}P$(p, \gamma)^{29}$S rate by using the contributions from narrow and isolated resonances, rather than by the statistical model used in previous works (Rauscher & Thielemann 2000; Cyburt et al. 2010; Sallaska et al. 2013). In addition, considering the realistic stellar evolution scenario, the effect of the thermally populated excited states of target nuclei should also be considered. The new reaction rate includes the contribution from proton capture on the first excited state of ^{28}P at 105.64 keV. With the new rate, we also explore its impact on the nucleosynthesis process in ONe novae.

The paper is structured as follows. Section 2 introduces the basic formalism for astrophysical reaction-rate calculations. We derive the new reaction rate for ^{28}P$(p, \gamma)^{29}$S, including both the contribution from ground-state and first-excited state capture, in Sect. 3. In Sect. 4, we investigate the impact of the new rates on the nova nucleosynthesis when using the 1D hydrodynamic code SHIVA. The conclusions are discussed in Sect. 5.

2. ^{28}P$(p, \gamma)^{29}$S reaction rate

2.1. Shell model calculation

The ^{29}S energy structure information currently remains unknown, except the ground state and the other five excited states at 1222 keV, 1727 keV, 2887 keV, 7.4 MeV, and 10 MeV (Shamsuzzoha Basunia 2012). However, none of these excited states resides in the energy region of nova interest. Furthermore, the energy levels of its mirror nucleus ^{29}Al obtained from the β^- decay of ^{29}Mg by Guillemaud-Mueller et al. (1984) are poorly understood; the assignment of spin and parity and the branching ratios of γ transitions for the specific excited states are still not confirmed, with only upper limits provided. The spectroscopic factors of proton emission for our target states used to calculate the resonant rates are also unknown. It is reported that the shell model can guarantee the typical uncertainty of around 100 keV in level energies for the *sd*-shell nuclei (Brown & Wildenthal 1988; Herndl et al. 1995). Therefore, we performed a shell-model calculation to derive the energy structure information used to calculate the resonant reaction rates. We calculate the ^{29}S energy levels using the KSHELL shell-model code (Shimizu et al. 2019) and the *sd*-shell-model space involving the $\pi 0d_{5/2}$, $\pi 0d_{3/2}$, $\pi 1s_{1/2}$, $\nu 0d_{5/2}$, $\nu 0d_{3/2}$, and $\nu 1s_{1/2}$ valence orbits. Here, π denotes the proton and ν denotes the neutron. The new isospin-breaking USDC interaction was used in the present work (Magilligan & Brown 2020). The calculated results on the energy levels of ^{29}S and the mirror nucleus ^{29}Al are shown in Fig. 1. For comparison, the available experimental energy levels of this pair of mirror nuclei are also added. We can see that the energy levels of ^{29}Al predicted by the shell-model match closely

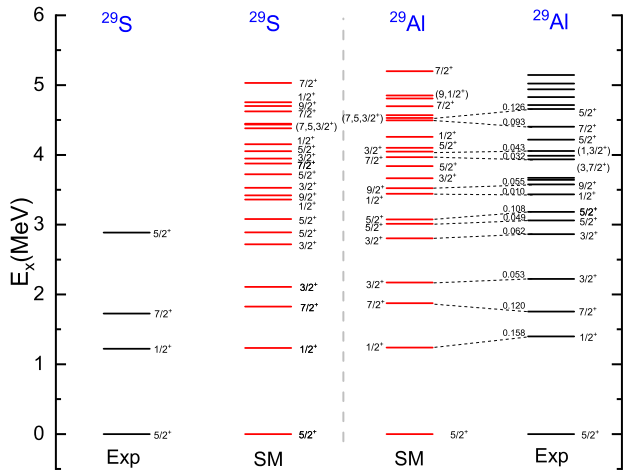

Fig. 1. Comparison of experimental and theoretical excitation energies for mirror nuclei ^{29}S and ^{29}Al, where "SM" is the result of the Shell-model, and "Exp" is the result from the experiment. The numbers on the dashed lines represent the energy level differences in megaelectronvolt for the corresponding energy levels.

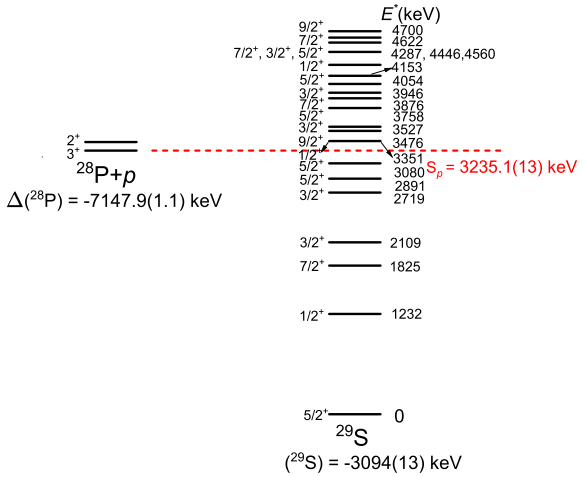

Fig. 2. Simplified level scheme of ^{29}S. The drawing is not to scale. The mass excesses and single proton separation energy (S_p) are from AME2020 (Wang et al. 2021), whereas the energies of the excited states are from the shell-model calculation.

the experimental result. The other critical information used to calculate the resonant reaction rates, such as reduced transition probabilities $B(M1)$ and $B(E2)$ and the spectroscopic factor of ^{28}P$(p, \gamma)^{29}$S, are also obtained through the shell model.

2.2. Reaction-rate calculation

The thermonuclear ^{28}P$(p, \gamma)^{29}$S reaction rate can be calculated as the incoherent sum of all resonant and nonresonant capture contributions. It is well known that only the resonances located in the energy window of astrophysical interest (called the Gamow window) significantly contribute to the reaction rate. For isolated narrow resonances, the resonant reaction rate for capture on a nucleus in an initial state i can be calculated as a sum over all relevant compound nucleus states j above the proton threshold (Fowler & Hoyle 1964; Hou et al. 2023b):

$$N_{\rm A}\langle\sigma\nu\rangle_{res,i} = 1.5394\times10^{11}\times(\mu T_9)^{-3/2}\times\sum_j \omega\gamma_{ij} \times\exp\left(-\frac{E_{ij}}{kT}\right)({\rm cm^3\ s^{-1}\ mol^{-1}}), \quad (1)$$

where $N_{\rm A}$ is Avogadro's constant, μ is the reduced mass of the ^{28}P+p system in atomic mass units, T_9 is the temperature in gigakelvin (GK), and k is the Boltzmann constant. The resonance energy in the center-of-mass system, $E_{ij} = E_j - Q - E_i$, is calculated from the excitation energies of the initial E_i and compound nucleus E_j state, where the resonance strengths $\omega\gamma_{ij}$ are given in units of MeV and can be calculated for proton capture as

$$\omega\gamma_{ij} = \frac{2J_j+1}{(2J_p+1)(2J_i+1)}\frac{\Gamma_{{\rm p}ij}\times\Gamma_{\gamma j}}{\Gamma_{{\rm tot}\,j}}, \quad (2)$$

where J_i is the spin of the target and $J_p = 1/2$ is the spin of a proton. J_j, $\Gamma_{{\rm p}ij}$ and $\Gamma_{\gamma j}$ are spin, proton and γ-decay width of the compound nucleus state j, respectively. The total width $\Gamma_{{\rm tot}\,j}$ is given by $\Gamma_{{\rm tot}\,j} = \Gamma_{{\rm p}ij} + \Gamma_{\gamma j}$. The proton width can be obtained from the proton spectroscopic factor multiplied by the single-particle proton width $\Gamma_{{\rm sp}ij}$, as $\Gamma_{{\rm p}ij} = C^2S_{ij}\Gamma_{{\rm sp}ij}$ (Iliadis 1997).

The γ-decay widths are obtained from electromagnetic reduced transition probabilities $B(\Omega L; J_i \rightarrow J_f)$, where Ω stands for electric or magnetic, which carry the nuclear structure information of the resonance states and the final bound states. The reduced transition probabilities were computed within the framework of the shell model. The corresponding γ-decay widths for the most contributed transitions ($M1$ and $E2$) can be expressed as Herndl et al. (1995)

$$\Gamma_{M1}[eV] = 1.16\times10^{-2}E_\gamma^3[{\rm MeV}]B(M1)[\mu_N^2], \text{ and}$$
$$\Gamma_{E2}[eV] = 8.13\times10^{-7}E_\gamma^5[{\rm MeV}]B(E2)[e^2fm^4]. \quad (3)$$

In a stellar plasma, the low-lying excited states of the target nucleus are thermally populated and might have considerable influence on the actual astrophysical reaction rate. Thus, the rate contribution from the first excited state of 105.64 keV in ^{28}P should also be taken into account. In this work, the mass excesses of ^{28}P and ^{29}S were taken from AME2020 (Wang et al. 2021), where the specific values are –7147.9 (1.1) keV and –3094 (13) keV, respectively. Then, the proton separation energy (S_p) is fixed at 3235.1 (13) keV, as marked in Fig. 2. For classical ONe nova explosions with a peak temperature of 4×10^8 K (Starrfield et al. 2016), the upper limit of the nova Gamow window is less than 485 keV. In other words, the reaction rate, which includes contributions from all excited states of ^{29}S with excitation energies below 3.72 MeV, is sufficient for the accurate simulation of nova nucleosynthesis. However, considering that this reaction may be used in another proton capture process that occurs in X-ray bursts, we include 13 energy levels above the threshold here to ensure that the reaction rate is also reliable for X-ray bursts, even those with an extreme peak temperature of 1.95×10^9 K (Schatz et al. 2001). Here, it needs to be clarified that not all energy levels of the above 13 states are from shell-model predictions. There are five resonant states in mirror nucleus ^{29}Al known experimentally, which are at 3.433 MeV ($1/2^+$), 3.577 MeV ($9/2^+$), 3.641 MeV ($5/2^+$), 4.403 MeV ($7/2^+$), and 4.656 MeV ($5/2^+$), respectively. For reliability, here we use the excitation energies of the corresponding five energy levels in ^{29}S obtained by adding the shell model's calculated level shift to the respective energy level of mirror states in ^{29}Al instead of

Table 1. Parameters for present ^{28}P$(p,\gamma)^{29}$S resonant-rate calculation.

E_x ^{29}S(MeV)	E_r(MeV)	J^π	l	$C^2S_{5/2}$	$C^2S_{1/2}$	$C^2S_{3/2}$	Γ_γ(eV)	Γ_p(eV)	$\omega\gamma$(MeV)
3.351	0.116	$1/2^+$	2	0.0015			6.51×10^{-2}	6.70×10^{-14}	9.57×10^{-21}
3.476	0.241	$9/2^+$	2	0.0000		0.6191	1.14×10^{-2}	1.64×10^{-05}	1.17×10^{-11}
3.527	0.292	$3/2^+$	2	0.0177		0.0046	2.54×10^{-2}	9.24×10^{-06}	2.64×10^{-12}
3.758	0.523	$5/2^+$	0	0.0071	0.0022	0.3854	3.08×10^{-2}	1.48×10^{01}	1.32×10^{-08}
3.876	0.641	$7/2^+$	0	0.0000	0.0003	0.0095	5.73×10^{-4}	2.41×10^{00}	3.27×10^{-10}
3.946	0.711	$3/2^+$	2	0.0461		0.2606	7.13×10^{-2}	2.60×10^{00}	1.98×10^{-08}
4.054	0.819	$5/2^+$	0	0.0070	0.1159	0.0241	1.41×10^{-2}	2.58×10^{02}	6.06×10^{-09}
4.153	0.918	$1/2^+$	2	0.0001			1.47×10^{-4}	7.41×10^{-3}	2.07×10^{-11}
4.287	1.052	$7/2^+$	0	0.0028	0.0177	0.2060	4.67×10^{-3}	2.32×10^{03}	2.67×10^{-09}
4.446	1.211	$3/2^+$	2	0.0242		0.0853	7.13×10^{-2}	6.54×10^{01}	2.04×10^{-08}
4.560	1.325	$5/2^+$	0	0.0088	0.0062	0.0166	5.75×10^{-2}	1.27×10^{03}	2.46×10^{-08}
4.622	1.387	$7/2^+$	0	0.0010	0.0015	0.0190	2.18×10^{-4}	1.10×10^{03}	1.25×10^{-10}
4.700	1.465	$9/2^+$	2	0.0142		0.0006	3.82×10^{-2}	3.22×10^{01}	2.73×10^{-08}
3.351	0.011	$1/2^+$	2	0.0276		0.0262	6.51×10^{-2}	3.92×10^{-54}	7.84×10^{-61}
3.476	0.136	$9/2^+$	2	0.0183			1.14×10^{-2}	2.38×10^{-11}	2.38×10^{-17}
3.527	0.187	$3/2^+$	0	0.0062	0.0921	0.2783	2.54×10^{-2}	2.27×10^{-05}	9.07×10^{-12}
3.758	0.418	$5/2^+$	0	0.0011	0.1432	0.1283	3.08×10^{-2}	1.00×10^{00}	1.79×10^{-08}
3.876	0.536	$7/2^+$	2	0.0038		0.0019	5.73×10^{-4}	3.21×10^{-03}	3.89×10^{-10}
3.946	0.606	$3/2^+$	0	0.0000	0.0406	0.1094	7.13×10^{-2}	2.24×10^{01}	2.84×10^{-08}
4.054	0.714	$5/2^+$	0	0.0006	0.0825	0.0528	1.41×10^{-2}	8.30×10^{01}	8.48×10^{-09}
4.153	0.813	$1/2^+$	2	0.0686		0.3820	1.47×10^{-4}	1.23×10^{01}	2.95×10^{-11}
4.287	0.947	$7/2^+$	2	0.0175		0.1254	4.67×10^{-3}	1.36×10^{01}	3.73×10^{-09}
4.446	1.106	$3/2^+$	0	0.0232	0.0103	0.0007	7.13×10^{-2}	4.79×10^{02}	5.60×10^{-10}
4.560	1.220	$5/2^+$	0	0.0134	0.0000	0.0010	5.75×10^{-2}	3.63×10^{02}	3.45×10^{-08}
4.622	1.282	$7/2^+$	2	0.0008		0.3455	2.18×10^{-4}	3.08×10^{02}	1.74×10^{-10}
4.700	1.360	$9/2^+$	2	0.0011			3.82×10^{-2}	1.46×10^{00}	3.72×10^{-08}

Notes. E_x, excitation energy; E_r, center-of-mass resonance energy; J^π, spin and parity; C^2S, spectroscopic factors; Γ_γ, γ-decay width; Γ_p, proton-decay width and $\omega\gamma$, resonance strength. The upper part is for ground-state capture; the lower part is for capture on the first excited state in ^{28}P.

the absolute prediction of the shell model. The remaining eight levels are taken from the shell-model calculation. The 13 energy levels above the proton threshold are shown in Fig. 2, and the relevant parameters for the ^{28}P$(p,\gamma)^{29}$S resonant rate calculation are summarized in Table 1. The upper part of the table is for ground-state capture, while the lower part is for capture on the first excited state in ^{28}P. Columns 5–7 refer to the spectroscopic factors of the corresponding $0d_{5/2}$, $1s_{1/2}$, and $0d_{3/2}$ orbits.

For the nonresonant reaction rate, it is directly related to the astrophysical S factor (S(E)) via the following expression (Rolfs & Rodney 1988; Iliadis 2015):

$$N_{\rm A}\langle\sigma\nu\rangle_{dc\,i} = 7.8327\times10^{9}\times\left(\frac{Z_pZ_T}{\mu T_9^2}\right)^{1/3}\times S_{i\,\rm eff} \times\exp\left[-4.2487\left(\frac{Z_p^2Z_T^2\mu}{T_9}\right)^{1/3}\right](\rm cm^3\,s^{-1}\,mol^{-1}), \quad (4)$$

where $S_{i\,\rm eff}$ can be parameterized by the formula

$$S_{i\,\rm eff}\approx S_i(0)\left[1+0.09807\left(\frac{T_9}{Z_p^2Z_T^2\mu}\right)^{1/3}\right], \quad (5)$$

and $S(0)$ is the sum of the individual S factors of the transitions from the initial state i into all bound states in the final nucleus; η is the Sommerfeld parameter.

The $S(0)$ for direct capture into the bound states of ^{29}S were calculated with a RADCAP code (Bertulani 2003) based on a Woods-Saxon nuclear potential (central + spin-orbit) and a Coulomb potential of a uniform charge distribution. The nuclear potential parameters were determined by matching the bound-state energies. The spectroscopic factors were calculated using the shell-model code calculation. Table 2 lists the individual S factors found for transitions into the seven bound states of ^{29}S from the ^{28}P ground state and the first excited state. Our uncertainty of $S(0)$ for direct capture is set to 42%. This includes not only an assumed uncertainty of 40%, as in Downen et al. (2022), but also the contribution due to uncertainty of the Q-value of 13 keV.

3. New reaction rate

In stellar plasma, the total reaction rate is the sum of the capture rate on all thermally excited states in the target nucleus weighted with their individual population factors (Fowler & Hoyle 1964; Schatz et al. 2005):

$$N_{\rm A}\langle\sigma\nu\rangle = \sum_i (N_{\rm A}\langle\sigma\nu\rangle_{res\,i} + N_{\rm A}\langle\sigma\nu\rangle_{dc\,i})\times\frac{(2J_i+1)e^{-E_i/kT}}{\sum_n(2J_n+1)e^{-E_n/kT}}. \quad (6)$$

In this work, we only considered capture on the ground state and the first excited state in ^{28}P, since the 885 keV energy of the

Table 2. Spectroscopic factors C^2S and astrophysical S factors $S(0)$ for direct capture into bound states in ^{29}S.

$E_x(MeV)$	J^π	$(nl_0)_{j0}$	C^2S	$S(0)$ (keV b)	C^2S^*	$S(0)^*$ (keV b)
0	$5/2^+$	$2s_{1/2}$	0.4606	31.46	0.3936	38.59
		$1d_{3/2}$	0.1352	0.7612	0.1520	1.234
		$1d_{5/2}$	0.0567	0.3440	0.0288	0.2481
1.232	$1/2^+$	$1d_{3/2}$			0.0796	0.1483
		$1d_{5/2}$	0.0627	0.0887	0.0090	0.0180
1.825	$7/2^+$	$2s_{1/2}$	0.0317	2.574		
		$1d_{3/2}$	0.5038	2.072	0.1902	1.125
		$1d_{5/2}$	0.0446	0.2085	0.0355	0.2429
2.109	$3/2^+$	$2s_{1/2}$			0.0071	0.4053
		$1d_{3/2}$			0.0411	0.1098
		$1d_{5/2}$	0.0277	0.0580	0.0330	0.1020
2.719	$3/2^+$	$2s_{1/2}$			0.0137	0.9193
		$1d_{3/2}$			0.0711	0.1418
		$1d_{5/2}$	0.0096	1.645×10^{-2}		
2.891	$5/2^+$	$2s_{1/2}$	0.1517	14.02	0.0230	2.519
		$1d_{3/2}$	0.1590	0.3155	0.2961	0.8083
3.080	$5/2^+$	$2s_{1/2}$	0.0015	0.1370	0.0029	0.3894
		$1d_{3/2}$	0.0001	1.608×10^{-4}	0.0012	2.945×10^{-3}
		$1d_{5/2}$	0.0008	1.334×10^{-3}	0.0018	4.902×10^{-3}
Total				52.06		47.01

Notes. Listed are results for capture on the ^{28}P ground state as well as on the first excited state in ^{28}P (denoted with an asterisk). J^π are spin and parity of the ^{29}S final state, n is the node number, l_0 is the single-particle orbital momentum, and j_0 is the total single-particle angular momentum.

second excited state is too high to have an effective influence on the reaction rate. The ground state is experimentally known to have spin and parity 3^+. However, the spin and parity assignment of the experimentally known first excited state at 105.64 keV have not been confirmed. For the calculation of the reaction rate, we assign a spin parity of 2^+ based on the comprehensive consideration of both the level structure of the mirror nucleus ^{28}Al and our shell-model calculations.

The resonance energy uncertainty used in our evaluation is 158.5 keV, mainly contributed by the uncertainty in excited state energy of the 158 keV, which is thought to be the maximum energy difference between the shell-model prediction and the experimental measurements for an arbitrary state below 5.0 MeV in mirror nucleus ^{29}Al. The gamma width uncertainties are uniformly assumed to be a factor of three, as in Hou et al. (2023a). For the spectroscopic factor C^2S predicted from the shell model, we assign a corresponding uncertainty factor of 2, 5, 10 for cases of $C^2S > 0.2$, $0.01 \leq C^2S \leq 0.2$, and $C^2S < 0.01$, respectively. Using the resonance and the direct reaction information introduced above, the reaction rate and associated upper and lower limits can be consistently obtained by Monte Carlo sampling of all corresponding uncertainties in the resonance energy, spectroscopic factor, and gamma transition width (Longland et al. 2010; Iliadis et al. 2010a,b,c). Table 3 is for the ground-state capture, and Table 4 is for capture on the first excited state in ^{28}P.

The first excited state rate is overall larger than the ground-state rate, and the maximum difference is up to two orders of magnitude, as shown in Fig. 3. We also plot the fractional contributions of different resonances to the reaction rate in Figs. 4 (capture on the ground state) and 5 (capture on the first excited state). For ground-state capture, the resonant rate at $0.03 < T_9 < 2$ is dominated by the resonances at E_r =241 and 523 keV, and the resonances at 292 keV and 711 keV also make a substantial contribution in a certain temperature region. The direct reaction contribution dominates for temperatures below 0.03×10^9 K. The rate contribution for capture on the first excited state is mostly from three resonances at E_r = 187, 418, and 606 keV for the temperature range of 0.02×10^9–2×10^9 K.

After taking into account the effect of the thermally excited state population by Eq. (6), the final reaction rate can be obtained as listed in Table 5. Figure 6 shows the new total rate of ^{28}P$(p, \gamma)^{29}$S and the associated uncertainties. For comparison, the previous rates collected in the Joint Institute for Nuclear Astrophysics Reaction Library (JINA REACLIB) database from Rauscher & Thielemann (2000), Cyburt et al. (2010), and Wallace & Woosley (1981), and the latest one proposed in STARLIB (Sallaska et al. 2013) (hereafter rath, ths8, wawo, and starlib, respectively), are also added. Our result is, overall, larger than the wawo rate, except for the narrow temperature interval of 0.17×10^9–0.26×10^9 K. Compared with the statistical model rates, our new rate shows different patterns of discrepancy from each one of them (ths8, rath, starlib) over the temperature range $T < 1 \times 10^8$ K, and the largest difference is over four orders of magnitude. HF rate predictions are expected to behave worse in a low temperature zone because of the lower nuclear level density close to the threshold. However, for temperatures from 1×10^8 K to 1.1×10^9 K, which covers the entire temperature region of nova interest, our rate agrees with the previous HF rates within uncertainties, indicating that the statistical model is a reasonable approximation for the prediction of the ^{28}P$(p, \gamma)^{29}$S rate in this temperature region. For temperatures $\geq 1.1 \times 10^9$ K, which are suitable for X-ray bursts, the statistical model rates are about a factor of two above our high rate.

The new rate in units of cm^3 mol^{-1} s^{-1} can be fitted (less than 3% error in 0.01–10×10^9 K) by the following

Table 3. New reaction rate for the ground-state capture for the ^{28}P(p, γ)^{29}S.

T (GK)	Low	Median	High	u.f.
0.100	5.544E-14	9.608E-12	3.566E-10	5.028E+01
0.200	1.631E-07	5.179E-06	3.414E-05	1.774E+01
0.250	5.788E-06	1.122E-04	7.643E-04	1.343E+01
0.300	7.308E-05	1.045E-03	6.960E-03	1.088E+01
0.400	2.329E-03	2.100E-02	1.343E-01	7.867E+00
0.500	2.243E-02	1.448E-01	7.876E-01	6.058E+00
0.600	1.127E-01	5.582E-01	2.571E+00	4.915E+00
0.700	3.600E-01	1.520E+00	6.045E+00	4.167E+00
0.800	8.837E-01	3.248E+00	1.138E+01	3.656E+00
0.900	1.814E+00	5.858E+00	1.872E+01	3.294E+00
1.000	3.186E+00	9.482E+00	2.798E+01	3.026E+00
1.250	8.925E+00	2.249E+01	5.679E+01	2.595E+00
1.500	1.757E+01	3.978E+01	9.101E+01	2.342E+00
1.750	2.866E+01	5.963E+01	1.289E+02	2.176E+00
2.000	4.097E+01	8.007E+01	1.674E+02	2.058E+00
2.500	6.745E+01	1.224E+02	2.374E+02	1.904E+00
3.000	9.415E+01	1.621E+02	2.986E+02	1.809E+00
3.500	1.181E+02	1.971E+02	3.513E+02	1.748E+00
4.000	1.382E+02	2.257E+02	3.924E+02	1.707E+00
5.000	1.668E+02	2.668E+02	4.487E+02	1.661E+00
6.000	1.831E+02	2.880E+02	4.785E+02	1.636E+00
7.000	1.902E+02	2.964E+02	4.883E+02	1.623E+00
8.000	1.920E+02	2.973E+02	4.872E+02	1.616E+00
9.000	1.896E+02	2.930E+02	4.778E+02	1.614E+00
10.000	1.833E+02	2.846E+02	4.658E+02	1.611E+00

Notes. In units of cm^3 mol^{-1} s^{-1}. Columns 2, 3, and 4 list the 16th, 50th, and 84th percentiles of the total rate probability density at given temperatures, respectively; u.f. is the uncertainty factor based on Monte Carlo sampling of the total reaction rate. The total number of samples at each temperature was 10 000.

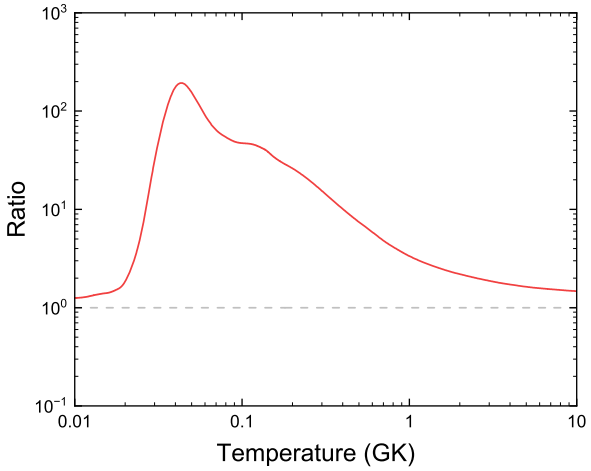

Fig. 3. Ratio of first excited state capture rate to that from the ground-state capture.

analytic expression, using the standard seven-parameter REACLIB format:

$$N_A\langle\sigma v\rangle = \exp(66.3299 - 1.1188T_9^{-1} + 11.9636T_9^{-1/3} - 79.8515T_9^{1/3} + 4.75799T_9 - 0.256103T_9^{5/3} + 30.5564\ln T_9)$$

Table 4. New reaction rate for capture on the first excited state in ^{28}P for the ^{28}P(p, γ)^{29}S.

T (GK)	Low	Median	High	u.f.
0.100	2.229E-12	4.517E-10	1.705E-08	8.374E+01
0.200	1.459E-06	1.366E-04	7.320E-04	2.397E+01
0.300	5.611E-04	1.610E-02	6.447E-02	1.163E+01
0.400	1.664E-02	2.115E-01	7.282E-01	7.294E+00
0.500	1.390E-01	1.073E+00	3.377E+00	5.357E+00
0.600	5.767E-01	3.294E+00	9.576E+00	4.330E+00
0.700	1.628E+00	7.278E+00	2.027E+01	3.721E+00
0.800	3.475E+00	1.342E+01	3.521E+01	3.328E+00
0.900	6.297E+00	2.157E+01	5.462E+01	3.056E+00
1.000	1.006E+01	3.157E+01	7.746E+01	2.858E+00
1.250	2.346E+01	6.345E+01	1.448E+02	2.536E+00
1.500	4.124E+01	1.005E+02	2.174E+02	2.339E+00
1.750	6.174E+01	1.388E+02	2.906E+02	2.203E+00
2.000	8.303E+01	1.755E+02	3.570E+02	2.102E+00
2.500	1.266E+02	2.448E+02	4.776E+02	1.962E+00
3.000	1.659E+02	3.035E+02	5.677E+02	1.872E+00
3.500	2.002E+02	3.504E+02	6.397E+02	1.812E+00
4.000	2.262E+02	3.885E+02	6.935E+02	1.771E+00
5.000	2.608E+02	4.337E+02	7.537E+02	1.719E+00
6.000	2.769E+02	4.535E+02	7.780E+02	1.692E+00
7.000	2.802E+02	4.563E+02	7.748E+02	1.677E+00
8.000	2.777E+02	4.501E+02	7.574E+02	1.666E+00
9.000	2.705E+02	4.361E+02	7.304E+02	1.661E+00
10.000	2.606E+02	4.200E+02	6.998E+02	1.657E+00

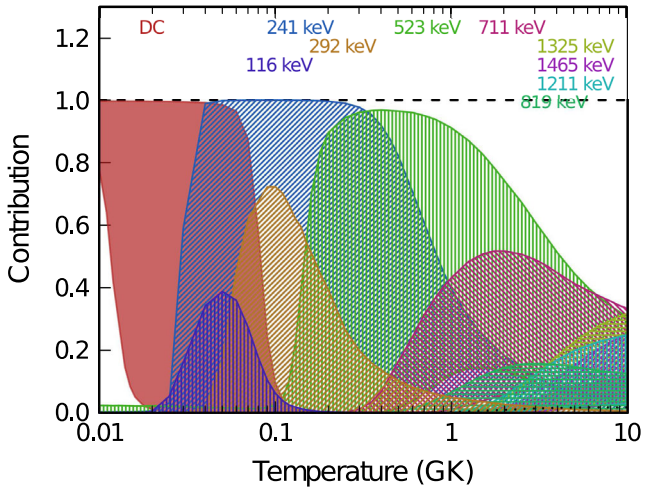

Fig. 4. Fractional contributions to the total ^{28}P(p, γ)^{29}S reaction rate. Resonances are labeled by their center-of-mass resonance energies, and the label "DC" refers to the direct capture process. The contribution ranges are shown as colored bands, with the band thickness representing the uncertainty of the contribution. Resonances that contribute less than 15% are not shown here.

$$+ \exp(-38.657 - 3.60937T_9^{-1} + 65.6321T_9^{-1/3} + 1.01158T_9^{1/3} - 27.0399T_9 + 4.0197T_9^{5/3} + 39.3449\ln T_9) + \exp(-20.3953 - 0.0130833T_9^{-1} - 26.2335T_9^{-1/3} + 67.7113T_9^{1/3} - 22.8041T_9 + 2.88872T_9^{5/3} - 7.4298\ln T_9). \quad (7)$$

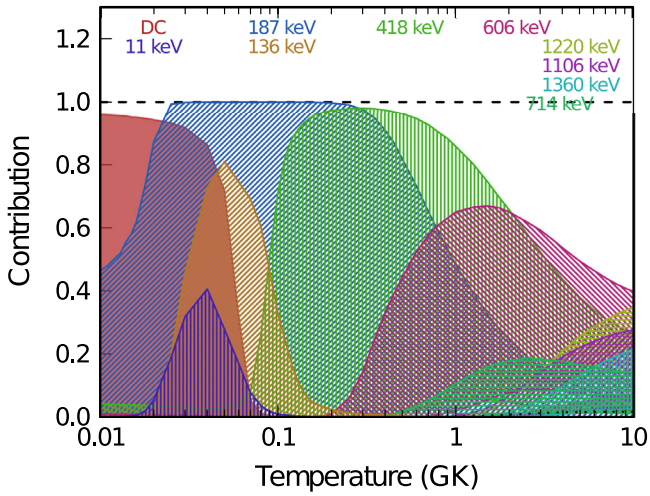

Fig. 5. Same as Fig. 4, but for capture on the first excited state of ^{28}P.

Table 5. Final new reaction rate for the ^{28}P(p, γ)^{29}S.

T (GK)	Low	Median	High	SEF
0.100	5.545E-14	9.610E-12	3.567E-10	1.00
0.200	1.652E-07	5.391E-06	3.526E-05	1.04
0.300	7.901E-05	1.228E-03	7.659E-03	1.18
0.400	2.799E-03	2.726E-02	1.538E-01	1.30
0.500	2.928E-02	1.994E-01	9.398E-01	1.38
0.600	1.525E-01	7.926E-01	3.171E+00	1.42
0.700	5.012E-01	2.161E+00	7.629E+00	1.42
0.800	1.233E+00	4.619E+00	1.459E+01	1.42
0.900	2.512E+00	8.305E+00	2.432E+01	1.42
1.000	4.385E+00	1.333E+01	3.661E+01	1.41
1.250	1.201E+01	3.118E+01	7.541E+01	1.39
1.500	2.327E+01	5.440E+01	1.214E+02	1.37
1.750	3.735E+01	8.042E+01	1.714E+02	1.35
2.000	5.274E+01	1.068E+02	2.224E+02	1.33
2.500	8.549E+01	1.597E+02	3.106E+02	1.30
3.000	1.173E+02	2.077E+02	3.854E+02	1.28
3.500	1.456E+02	2.485E+02	4.480E+02	1.26
4.000	1.686E+02	2.819E+02	4.963E+02	1.25
5.000	2.005E+02	3.267E+02	5.582E+02	1.22
6.000	2.176E+02	3.490E+02	5.888E+02	1.21
7.000	2.240E+02	3.564E+02	5.958E+02	1.20
8.000	2.246E+02	3.554E+02	5.899E+02	1.20
9.000	2.207E+02	3.480E+02	5.748E+02	1.19
10.000	2.132E+02	3.371E+02	5.564E+02	1.18

The stellar enhancement factor (SEF) is often used to describe the effect of the stellar medium on the actual capture rate relative to the ground-state capture rate obtained in the laboratory. Hence, SEF is defined as the ratio of the actual capture rate including thermal excitations of the target nucleus to the ground-state capture rate. We calculate the corresponding SEF at different temperatures caused by the first excited state capture in ^{28}P, as listed in the fifth column of Table 5. The first excited state capture has an obvious enhancement effect on the reaction rate over temperature region from 0.2×10^9 K to 10×10^9 K, even up to 40% around 1×10^9 K.

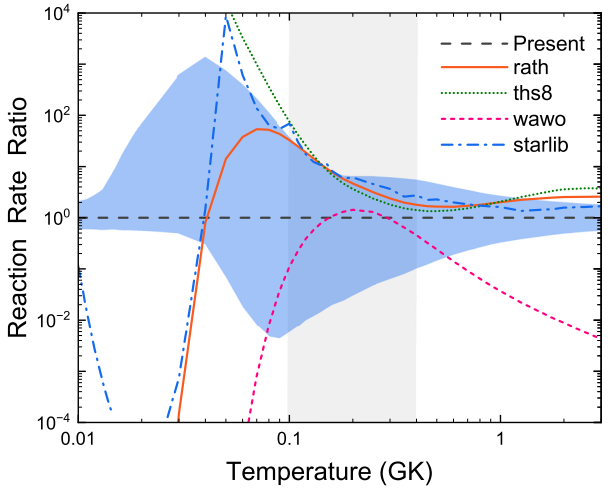

Fig. 6. Ratio of previous ^{28}P(p, γ)^{29}S rates normalized to present recommended rate (the median rates in Table 5). The different line patterns correspond to the rates from Rauscher & Thielemann (2000), Cyburt et al. (2010), Wallace & Woosley (1981), and Sallaska et al. (2013), as marked in rath, ths8, wawo, and starlib, respectively. The shallow blue shaded areas correspond to 68% coverage probabilities, labeled as "Low" and "High" in Table 5. The vertical shallow gray band indicates the typical temperature range of nova nuclear burning.

4. Astrophysical impact for classical nova

The impact of the new ^{28}P(p,γ)^{29}S rates on nova nucleosynthesis has been analyzed in a series of four simulations performed with the spherically symmetric, Lagrangian, 1-D hydrodynamic code SHIVA, which has been extensively used in the modeling of nova outbursts (José 2016; José & Hernanz 1998). SHIVA includes a general equation of state, with contributions from the degenerate electron gas, the ion plasma, and radiation. Coulomb corrections to the electron pressure component are taken into account, and both radiative and conductive opacities are considered in the energy transport. Nuclear-energy generation is determined by means of a reaction network that contains 120 species (ranging from ^{1}H to ^{48}Ti); this is linked through 630 nuclear processes with updated rates from the STARLIB database (Sallaska et al. 2013; Iliadis, 2013, priv. comm.). Matter accreted from the stellar companion, at a typical rate of 2×10^{-10} $M_\odot$ yr^{-1} is assumed to mix with material from the outermost layers of the underlying white dwarf to a characteristic level of 50% to match observations of ONe novae. In all the hydrodynamic simulations reported in this paper, a 1.35 $M_\odot$ ONe white dwarf, with an initial luminosity of ~0.01 $L_\odot$, has been adopted. All simulations are identical, except for the specific prescriptions adopted for the forward and reverse ^{28}P(p, γ)^{29}S rates: STARLIB rates were adopted in the first simulation; for the additional three simulations, low, recommended and high ^{28}P(p, γ)^{29}S, and ^{29}S(γ, p)^{28}P rates were used.

Table 6 summarizes the mean composition of ejecta, expressed in mass fractions of Si–Ca group elements, corresponding to three models computed with the newly established low, recommended, and high rates (Cols. 2–4). The simulations reveal that the adoption of the new rates does not substantially alter the abundance pattern of these isotopes when compared to the model computed with STARLIB rates, with differences amounting to less than 1.5%. The last column provides the percentage change in abundances between the simulations with upper and lower limits on the rates. Except for ^{28}Si, the

Table 6. Averaged mass fraction of ejecta (Si–Ca) from 1.35 $M_\odot$ ONe white-dwarf models.

Species	Lower	Recommend	Upper	$\lvert X_u - X_l\rvert/X_l$
^{28}Si	3.11E-02	3.10E-02	3.02E-02	2.89%
^{29}Si	2.42E-03	2.40E-03	2.40E-03	0.83%
^{30}Si	1.54E-02	1.54E-02	1.53E-02	0.65%
^{31}P	8.74E-03	8.73E-03	8.73E-03	0.11%
^{32}S	5.28E-02	5.30E-02	5.37E-02	1.71%
^{33}S	8.06E-04	8.14E-04	8.30E-04	2.98%
^{34}S	3.67E-04	3.71E-04	3.79E-04	3.27%
^{35}Cl	3.93E-04	3.98E-04	4.07E-04	3.56%
^{36}S	1.56E-09	1.61E-09	1.58E-09	1.28%
^{36}Ar	5.24E-05	5.33E-05	5.45E-05	4.01%
^{37}Cl	1.47E-04	1.49E-04	1.52E-04	3.40%
^{38}Ar	2.45E-05	2.47E-05	2.49E-05	1.63%
^{39}K	6.06E-06	6.07E-06	6.06E-06	0.00%
^{40}Ca	3.25E-05	3.25E-05	3.25E-05	0.00%

Notes. X_u and X_l indicate the isotope abundance using upper limits and lower limits of ^{28}P(p, γ)^{29}S, respectively.

most abundant Si–Ca nuclei – ^{32}S, ^{30}Si, ^{31}P, and ^{29}Si- are only marginally affected by the current uncertainties in the ^{28}P(p, γ)^{29}S and ^{29}S(γ, p)^{28} rates. The most significant impact is observed in ^{28}Si, ^{33,34}S, ^{35,37}Cl, and ^{36}Ar, with relative abundance variations at the level of 3% to 4%. It is important to emphasize that, while the new rates do not exert a significant influence on element production in novae, the uncertainty of these rates has now been significantly reduced. The present reaction rate is accurate enough, making novae nucleosynthesis predictions sound.

5. Conclusion

Accurate nuclear masses and excitation energies are crucial quantities for improving the accuracy of proton-capture reaction rates on short-lived and proton-rich nuclei. In this study, using the updated proton threshold of $S_p = 3235.1(13)$ keV determined by the ^{29}S new mass of high-accuracy, together with the energy structure information of ^{29}S by shell model, we recalculated the thermonuclear reaction rate of ^{28}P(p, γ)^{29}S and its associated uncertainty via a Monte Carlo method. In particular, we considered the contribution from the capture on the first excited state of ^{28}P for the first time. We find that the first excited state in ^{28}P at 105.6 keV has an enhancement effect of over 30% on the final reaction rate over the temperature range from 4×10^8 K to 2.5×10^9 K, which is not considered in previous evaluations. In comparison to the HF statistical model rates, it is found that our new rate shows different discrepancy patterns from the ths8, rath, and starlib rates in different temperature regions. Despite the fact that HF predictions cannot be safely used for the case of the compound nucleus with insufficient high-level densities, in this specific case we see that the new rate still agrees with those within uncertainties at typical nova temperatures.

To investigate the impact of the new reaction rates on the hydrogen burning that occurred in ONe novae, we performed a series of nucleosynthesis calculations in which four groups of different reaction rates of ^{28}P(p, γ)^{29}S were used. Compared with the result using previous starlib rates, it is found that the adoption of new rates has no significant effect on the final yields of intermediate-mass isotopes from Si to Ca produced in a 1.35 $M_\odot$ ONe nova explosion, and the largest differences are no larger than 1.5%. Comparing two simulations using upper and lower limits of reaction rates, we also find that the rate uncertainty of up to two orders of magnitude at typical nova temperatures has a limited impact on the final isotope abundance of the ejecta from ONe nova outburst. Nuclides with the largest changes in relative abundance are ^{28}Si, ^{33,34}S, ^{35,37}Cl, and ^{36}Ar, approximately at the level of 3%−4%.

Acknowledgements. This work was financially supported by the National Key R&D Program of China Grant No. 2022YFA1603300, Longyuan Youth Talent Program of Gansu Province, the Strategic Priority Research Program of Chinese Academy of Sciences Grant No. XDB34020204, and in part by the National Science Foundation under Grant No. OISE-1927130 (IReNA). J.J. acknowledges support from the MINECO grant PID2020-117252GB-I00, by the EU Feder funds, and by the AGAUR/Generalitat de Catalunya grant SGR-386/2021. C.A.B. acknowledges support by the U.S. DOE grant DE-FG02-08ER41533 and the Helmholtz Research Academy Hesse for FAIR. M.P. and TT acknowledge the ongoing access to `viper`, the University of Hull High Performance Computing Facility. J.J., M.P. and T.T. acknowledge the support of the European Union's Horizon 2020 research and innovation programme (ChETEC-INFRA – Project no. 101008324). M.P. acknowledges the support from the "Lendulet-2023" LP2023-10 Programme of the Hungarian Academy of Sciences (Hungary), and the support from the NKFI via K-project 138031 (Hungary). J.G.L. acknowledges support from the National Natural Science Foundation of China under Grants No. 12205340; the Gansu Natural Science Foundation under Grant No. 22JR5RA123. R.L. acknowledges support from the U.S. Department of Energy, Office of Science, Office of Nuclear Physics, under Award Number DE-SC0017799 and Contract Nos. DE-FG02-97ER41033 and DE-FG02-97ER41042.

References

Bellomo, M., Shore, S. N., & José, J. 2024, A&A, submitted
Bertulani, C. 2003, Comput. Phys. Commun., 156, 123
Brown, B. A., & Wildenthal, B. H. 1988, Annu. Rev. Nucl. Part. Sci., 38, 29
Casanova, J., José, J., Garcia-Berro, E., Shore, S., & Calder, A. 2011, Nature, 478, 490
Cyburt, R. H., Amthor, A. M., Ferguson, R., et al. 2010, ApJS, 189, 240
Downen, L. N., Iliadis, C., José, J., & Starrfield, S. 2012, ApJ, 762, 105
Downen, L. N., Iliadis, C., Champagne, A. E., et al. 2022, Phys. Rev. C, 105, 055804
Fowler, W. A., & Hoyle, F. 1964, ApJS, 9, 201
Gehrz, R. D., Truran, J. W., Williams, R. E., & Starrfield, S. 1998, PASP, 110, 3
Guillemaud-Mueller, D., Detraz, C., Langevin, M., et al. 1984, Nucl. Phys. A, 426, 37
Herndl, H., Görres, J., Wiescher, M., Brown, B. A., & Van Wormer, L. 1995, Phys. Rev. C, 52, 1078
Hou, S. Q., Iliadis, C., Pignatari, M., et al. 2023a, A&A, 677, A139
Hou, S. Q., Liu, J. B., Trueman, T. C. L., et al. 2023b, ApJ, 950, 133
Iliadis, C. 1997, Nucl. Phys. A, 618, 166
Iliadis, C. 2015, Nuclear Physics of Stars, 2nd edn. (Weinheim: Wiley-VCH Verlag)
Iliadis, C., Champagne, A., José, J., Starrfield, S., & Tupper, P. 2002, ApJS, 142, 105
Iliadis, C., Longland, R., Champagne, A., & Coc, A. 2010a, Nucl. Phys. A, 841, 251
Iliadis, C., Longland, R., Champagne, A., & Coc, A. 2010b, Nucl. Phys. A, 841, 323
Iliadis, C., Longland, R., Champagne, A., Coc, A., & Fitzgerald, R. 2010c, Nucl. Phys. A, 841, 31
José, J. 2016, Stellar Explosions: Hydrodynamics and Nucleosynthesis (Boca Raton, FL: CRC/Taylor and Francis)
José, J., & Hernanz, M. 1998, ApJ, 494, 680
José, J., & Shore, S. N. 2008, in Classical Novae, eds. M. F. Bode, & A. Evans, 2nd edn. (Cambridge, UK: Cambridge University Press), 121
José, J., Coc, A., & Hernanz, M. 2001, ApJ, 560, 897
José, J., Hernanz, M., & Iliadis, C. 2006, Nucl. Phys. A, 777, 550
José, J., Halabi, G. M., & El Eid, M. F. 2016, A&A, 593, A54
José, J., Shore, S. N., & Casanova, J. 2020, A&A, 634, A5
Longland, R., Iliadis, C., Champagne, A., et al. 2010, Nucl. Phys. A, 841, 1

Magilligan, A., & Brown, B. A. 2020, Phys. Rev. C, 101, 064312
Rauscher, T., & Thielemann, F.-K. 2000, At. Data Nucl. Data Tables, 75, 1
Rolfs, C. E., & Rodney, W. S. 1988, Cauldrons in the Cosmos (Chicago: University of Chicago Press)
Sallaska, A. L., Iliadis, C., Champange, A. E., et al. 2013, ApJS, 207, 18
Schatz, H., Aprahamian, A., Barnard, V., et al. 2001, Phys. Rev. Lett., 86, 3471
Schatz, H., Bertulani, C. A., Brown, B. A., et al. 2005, Phys. Rev. C, 72, 065804
Shafter, A. W. 2017, ApJ, 834, 196
Shamsuzzoha Basunia, M. 2012, Nucl. Data Sheets, 113, 909
Shimizu, N., Mizusaki, T., Utsuno, Y., & Tsunoda, Y. 2019, Comput. Phys. Commun., 244, 372
Starrfield, S., Iliadis, C., & Hix, W. R. 2008, in Classical Novae, eds. M. F. Bode, & A. Evans (Cambridge: Cambridge University Press), 43, 77
Starrfield, S., Iliadis, C., & Hix, W. R. 2016, PASP, 128, 051001
Wallace, R. K., & Woosley, S. E. 1981, ApJS, 45, 389
Wang, M., Huang, W. J., Kondev, F. G., Audi, G., & Naimi, S. 2021, Chin. Phys. C, 45, 030003